Journal of Sound and Vibration (1998) **214**(5), 853–871
Article No. sv981590

IDENTIFICATION OF A NON-LINEAR ELECTROMAGNETIC SYSTEM: AN EXPERIMENTAL STUDY

S.-C. CHANG AND P.-C. TUNG

Department of Mechanical Engineering, *National Central University*, *Chung-Li*, *Taiwan* 32054, *Republic of China*

(*Received* 5 *June* 1997, *and in final form* 5 *February* 1998)

This paper is concerned with the technique of identifying a non-linear electromagnetic system experimentally based on the principle of harmonic balance and the curve fitting method. The system under investigation is a symmetric rotor suspended by a spring device and excited by an electromagnet of a magnetic bearing. Particular emphases are placed on the identifiability of such a technique for this system and how to improve the modelling accuracy. The traditional identification technique is modified in order to successfully identify this system possessing highly non-linear characteristics. The resulting non-linear model has been proven to be in agreement with the experimental data. The knowledge gained from these studies are presented and discussed thoroughly.

1. INTRODUCTION

In industrial applications, magnetic bearings are superior to conventional bearings in performances such as high rotation speed, no friction, and high precision. When used, one expects that the rotor suspended by the magnetic bearing rotates stably through the rotating speeds. This requires a closed loop control to stabilize the system and to eliminate vibrations due to disturbed forces.

The characteristics of magnetic bearings are inherently non-linear due to the non-linearities of the electromagnetic forces. In a linear case study, the electromagnetic force is linearized about the operating point and considered to be a linear function of currents and air gaps. However, the linear relationship only holds locally. In practice, the electromagnetic forces are non-linear. When higher magnetic flux densities are used for reducing the weight and size of magnetic bearing or when a considerably large deviation of a spinned rotor is unavoidable due to large unbalance forces, the non-linear characteristics become quite significant. To accurately control or predict the performance of the system, the effects of these non-linearities should be taken into consideration. Generally, analytical and numerical techniques can be applied for this purpose. Numerical techniques such as the FEM model [1] may agree well with experiments if the mesh division is reasonable, but it takes much effort and calculation. Likewise, analytical techniques require the solving of the full set of Maxwell equations coupled with the kinetic equation for the rotor [2], and so are also quite difficult and complicated. One of the motivations for the present study is to consider whether the analysis can be simplified by applying a simple identification technique to search for the simplest mathematical model that can capture the dynamic behaviours of an electromagnetic system.

0022–460X/98/300853 + 19 $30.00/0

The problem of system identification is generally referred to as the determination of a mathematical model for a system or a process by observing its input–output relations. There are a number of well-known parameter identification techniques that have been successfully applied to the many cases. They include the method of maximum likelihood [3], least squares [4], and instrumental variable [5], etc. But most of the techniques developed so far cannot be applied to non-linear systems. Recently, the identification of a non-linear vibratory system is being further developed, and several techniques have been proposed in references [6–10]. Yasuda *et al*. [11] applied the harmonic balance principle to identify a multi-degree-of-freedom system with smooth non-linearity. Following closely, Yasuda *et al*. [12] extended this technique to systems containing non-smooth non-linearity. In the above studies, the identification techniques were proven to be applicable to their numerical examples, but experimental works have not been carried out.

As for the experimental identification, many efforts have been made, for example, the work studied by Wang *et al*. [13], Zhang *et al*. [14] and Arumugam *et al*. [15]. But those studies have only dealt with the problems of identifying linear experimental systems. Yi *et al*. [16] have proposed an identification method based on a sliding observer and a least square method. This method has been used to accurately identify the parameters of their half car suspension test rig. Zhang *et al*. [17] have also studied the problem of identification for a non-linear system. They developed the frequency domain method for estimating the unknown parameters in linear-in-the-parameter and non-linear systems. Their application for squeeze-film dampers has also proven to be very successful. But the method is only able to be used in smaller excited amplitudes and the excited frequencies are limited in a narrow-band. In these two experimental studies, the non-linear terms should be derived from theoretical calculation and values of parameters were unknown and needed to be identified.

Since the actual form of non-linear magnetic force may not be easily derived in practice, in this paper, the non-linear magnetic force is expressed by the form of polynomial, as in references [11, 18]. In practice, however, how many terms and how high the order should be set in the polynomial to fit a physical system is still a difficult decision. Theoretically, the technique described by references [11, 18] can allow one to assume a polynomial containing many homogenous non-linear terms up to a certain higher order and the calculations will lead the coefficients of all unnecessary terms to zero. However, since the data obtained by experiment may contain noise, the resulting coefficients of the unnecessary terms may not go to zero. Furthermore, errors may be introduced because too many terms are used in the calculations. Under this situation, the application of curve fitting will be of assistance to obtain the non-linear model. However, since the magnetic force is a function of both the air gap and the current, it is difficult to obtain a surface equation representing the magnetic force by merely applying the curve fitting. Thus, one first applies the curve fitting to fit the experimental data for fixed air gap and fixed current, which will result in the function representing the magnetic force that is a function of both the air gap and the current. These functions are combined and the harmonic balance method is applied to obtain the approximating non-linear equation for the magnetic force. The resulting model will be able to predict the dynamic behaviour quite well.

2. EXPERIMENTAL EQUIPMENT AND RESULTS

The magnetic bearing system shown in Figure 1 is chosen here for the analysis. The mechanical construction consists of an unload symmetric rotor which is attached to a flexible coupler at one end and supported by four radial electromagnets at the other end. This is a typical example of magnetic bearing systems. To simplify the analysis, the rotor

is kept unrotated and only one of the four electromagnets is used to apply harmonic force to the rotor to investigate the effects of its non-linear characteristics. Although this system looks simple, it possesses rich dynamics as will be seen later.

Two eddy current-type displacement sensors with sensitivity 1·0 V/mm are placed at the disk end. Two current transducers with sensitivity 1·0 V/A are used to measure the current in the electromagnetic coil. The input to the power amplifier is the forcing voltage ($A_0 \sin \omega t$) generated by a programmable function generator to act as an identification input signal.

In performing the experiment (see Figure 2(a)), a spring set and a bias voltage are applied to levitate the rotor at the centre position and one of the four electromagnets is used to excite the system by a series of harmonic forces. The output signals measured from displacement sensors and current sensors together with the forcing voltage are then recorded simultaneously by a personal computer with sampling time at 0·0001 s. Figure 2(b) shows the overall block diagram for this system.

In order to examine the steady state behaviour of the system, it is useful to plot the frequency response diagram showing how the maximum displacement amplitude (y_m) of the rotor will vary with various forcing frequency (ω). It is obtained by superimposing sinusoidal inputs on the bias voltage for our system. Figure 3 shows the frequency responses of the rotor displacement for input amplitude $A_0 = 3{\cdot}0$ V by decreasing forcing frequency (ω) from 80 to 34·4 Hz. If the system starts at high frequency, and then one

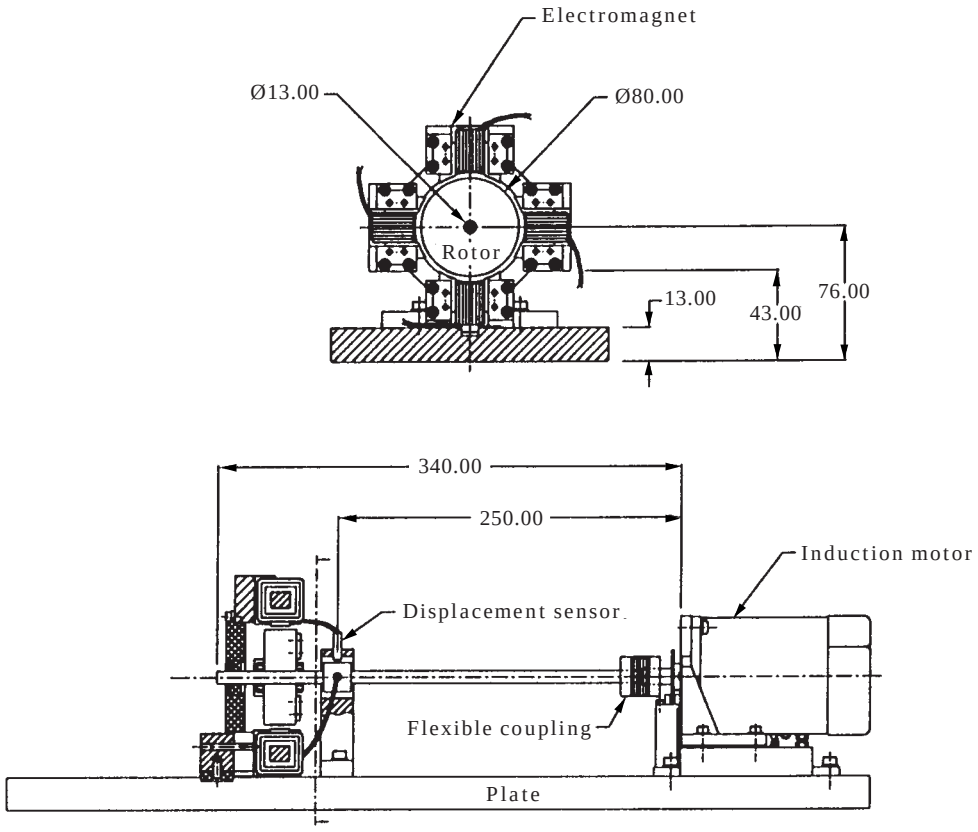

Figure 1. The magnetic bearing system (unit: mm).

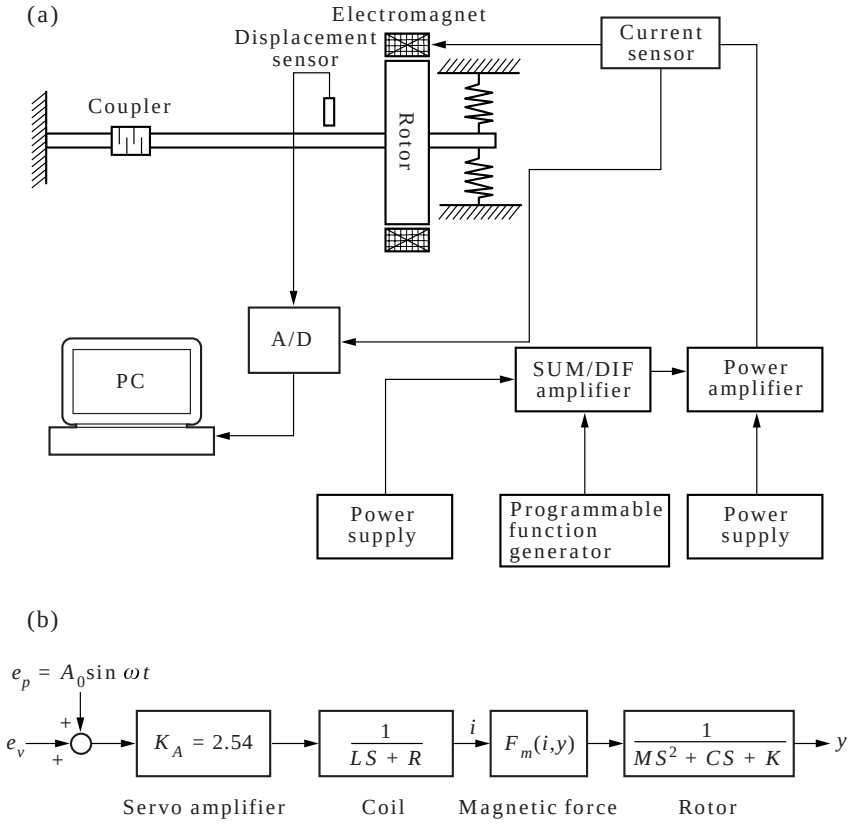

Figure 2. (a) The experimental set-up of the electromagnetic system. (b) An overall block diagram of this system.

slowly decreases the forcing frequency, there is an increase in amplitude along the resonant part of the response curve. The smooth variation of amplitude and frequency continues until near $\omega = 37{\cdot}6$ Hz, where the first period-doubling bifurcation occurs. In the period-doubling bifurcations, one starts with a system with a fundamental period motion. Then as experimental parameter (ω) is varied, the motion undergoes a bifurcation or change to a periodic motion with twice the period of the original oscillation. In other words, the motion of period $T(T = 2\pi/\omega)$ loses its stability and becomes a period $2T$ subharmonic oscillation. The stationary transitions from T to $2T$, from $2T$ to $4T$, . . . , etc. branches at the cascade bifurcation. Due to the fact that the identified system of our model is a soft-spring type system, usually the period doubling bifurcation phenomenon occurs in the neighbourhood of the resonant region for the soft-spring type system. Beyond this point, the vibrating amplitude of the rotor and the coil current grow sharply. As the forcing frequency continues to decrease, the trajectory continues to experience period-doubling bifurcations which eventually results in a chaotic motion; it was observed that the rotor strikes the electromagnet, i.e., the system is blown up. The bifurcation sequence is easily seen in the time series shown in Figure 4, which are recorded by a digital oscilloscope (Fluke 97) and the bias values have been removed. The spectrum, as shown in Figure 5, also shows the bifurcations with the presence of new frequency components at $\omega/2$, $3\omega/2$, $5\omega/2$, etc.

It was observed that the dynamics of the system are fairly complex due to non-linearities. The mathematical model would be necessary for designing conventional controllers; otherwise the system performance may be acceptable only for some specific conditions due to the fact that the controller gains are usually obtained through trial and error and are only effective locally.

3. IDENTIFICATION METHOD

In this section, the identification method proposed by Yasuda *et al*. [11] is described briefly and further calculation details can be obtained from reference [11]. The basic procedures of this technique are as follows. (1) Deduce an appropriate mathematical model that can capture the dynamic characteristics of the physical system to be identified. The unknown non-linear terms are approximated by an appropriate form of polynomials. (2) Persistently excite the system by choosing a series of an appropriate periodic force with various frequencies. At the same time, record this periodic force input and the corresponding period steady state responses simultaneously. (3) Express the input force term and each term in the equation of motion including the non-linear terms in Fouries series. (4) Apply the principle of harmonic balance to yield

$$[\mathbf{A}]\{\mathbf{S}\} = \{\mathbf{Q}\}, \tag{1}$$

where the matrix [**A**] is known and is constructed by the Fourier coefficients of all the terms in the equation of motion excluding that of the input force, vector $\{\mathbf{S}\}$ contains the unknown coefficients of the equation of motion to be determined, and vector $\{\mathbf{Q}\}$ is constructed by Fourier coefficients of the input force. Equation (1) can be solved using the weighted least-square method to obtain

$$\{\mathbf{S}\} = ([\mathbf{A}]^T[\mathbf{W}][\mathbf{A}]^{-1})[\mathbf{A}]^T[\mathbf{W}]\{\mathbf{Q}\}, \tag{2}$$

where the matrix [**W**] is the weighting matrix used to improve accuracy and $[\mathbf{A}]^T$ represents the transpose of matrix [**A**].

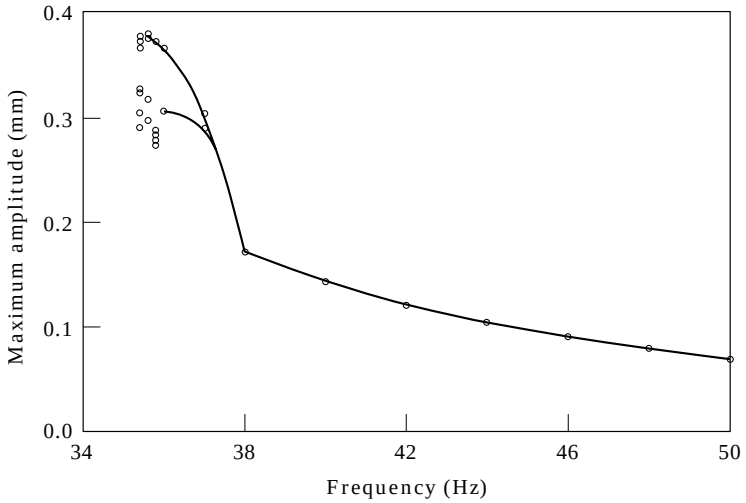

Figure 3. Bifurcation diagram obtained by the experiment (○ ○ ○).

4. SYSTEM IDENTIFICATIONS

The motion of the rotor is governed by

$$M\frac{\mathrm{d}^2y}{\mathrm{d}t^2} = -C\frac{\mathrm{d}y}{\mathrm{d}t} - Ky + F_m(i, y) + D, \tag{3}$$

where y is the oscillating displacement of the rotor about a reference point. Parameters C, K, and D denote the equivalent damping, stiffness and *dc* gain of the electromechanical system, respectively. F_m, the magnetic force of the electromagnet, is a function of the current and the air gap. It is noted that the term of *dc* gain is generated due to the origin of the chosen co-ordinate which may be different from the actual equilibrium point. In general, the calculation of this force is based on the field energy. If we neglect the iron losses and assume the electromagnet to be unsaturated, theoretically, this force is quadratically dependent on the current and inversely quadratically dependent on the air

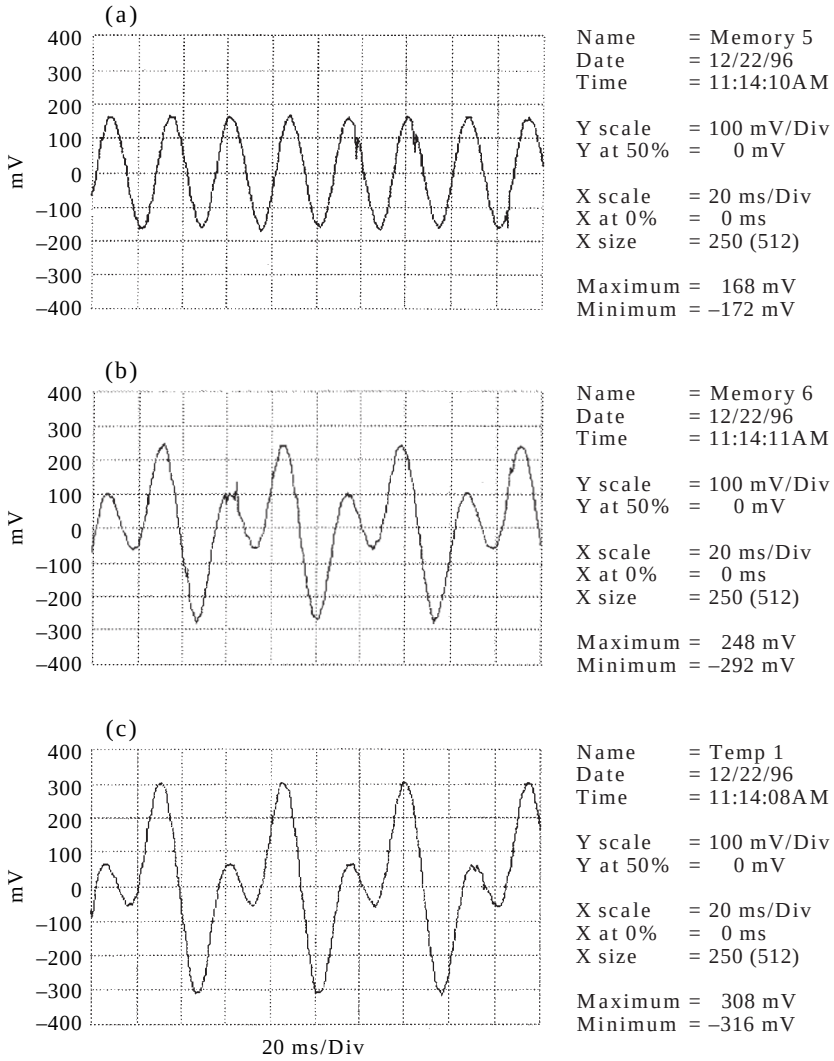

Figure 4. (a)–(d). *Caption opposite*

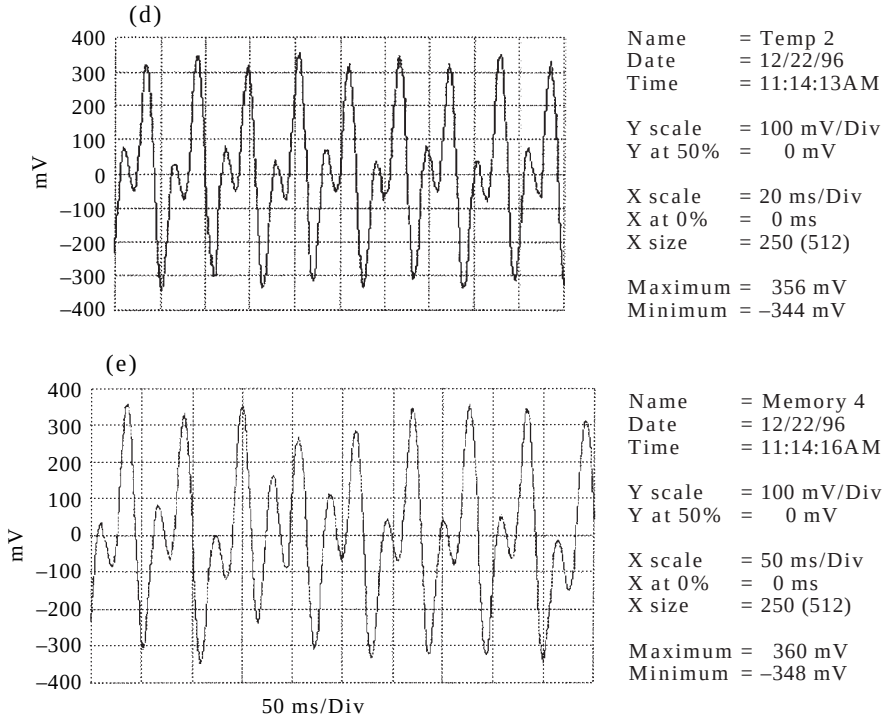

Figure 4. Development of time histories in transition to chaos at decreasing driving frequency. (a) $\omega = 37{\cdot}8$ Hz; (b) $\omega = 37{\cdot}6$ Hz; (c) $\omega = 36{\cdot}6$ Hz; (d) $\omega = 35{\cdot}6$ Hz; (e) $\omega = 35{\cdot}2$ Hz.

gap. However, if the iron of the electromagnet is operated beyond or close to saturation point with high flux densities (as in our case), one must consider the non-linear characteristics of the magnetization curve. Then, to determine exactly the motion of the rotor in the magnetic field requires the simultaneous solution to the full set of Maxwell equations coupled with the kinetic equation for the rotor. It is indeed a very difficult task, Thus, the non-linear magnetic force is approximated by an approximate form of polynomial in our study.

The equation of motion describing the response of current (i) is obtained from a voltage balance in the electromagnetic circuit. The disturbance voltage, $A_0 \sin \omega t$, is balanced by the voltage drop due to the resistance and the inductive reactance of the coil. The induced voltage in the coil is proportional to the number of turns (n) and the time rate of change of flux (Φ), i.e.,

$$n \frac{\mathrm{d}\Phi(i, y)}{\mathrm{d}t} + Ri = F_\Phi + Ri = K_A A_0 \sin \omega t, \tag{4}$$

where R is resistance of the coil and $K_A (= 2{\cdot}254)$ is the gain of the power amplifier. F_Φ represents the voltage drop due to the inductance and the back emf, which is a non-linear function of both the air gap and the current.

In the present work, the authors do not intend to determine exactly the form of F_Φ and F_m. Instead of following the general approaches, the analysis is simplified by applying the identification technique to find the simplest forms for F_Φ and F_m that can capture the dynamic behaviours of the physical system, especially in the neighbourhood of the bifurcation point shown in the experimental data.

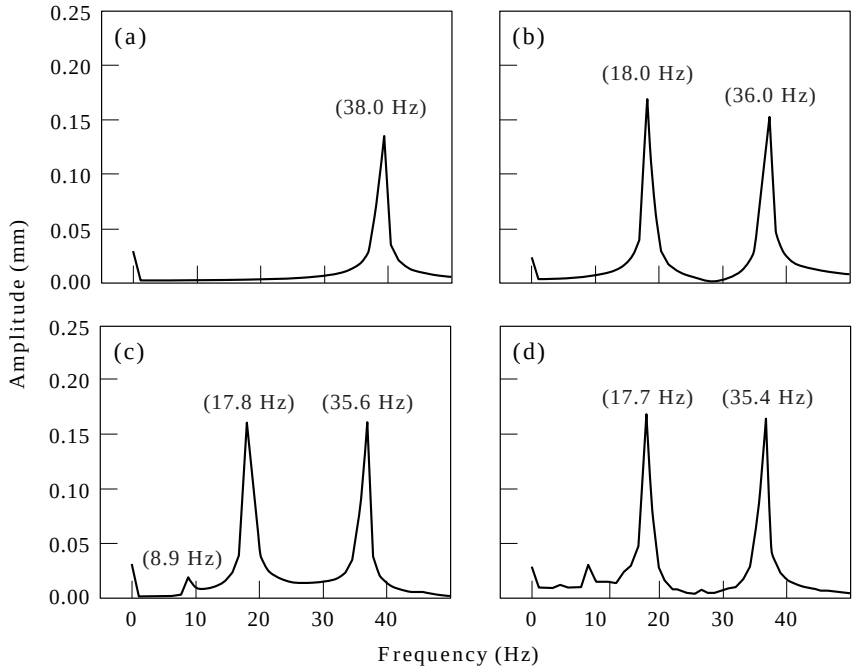

Figure 5. Frequency spectra evolutions of the experimental data. (a) The period-one solution; (b) the period-two solution; (c) the period-four solution; (d) the chaos motion.

In what follows, three cases are illustrated, from a simpler model to a complicated one. The experimental time series for $A_0 = 3{\cdot}0$ V and ω ranging from 38 to 80 Hz are employed to carry out the identification calculations with the assumption that up to the third order terms are retained up in the Fourier series expansion. In proceeding with the calculations, the weighting matrix in equation (2) is used to weight the data near the bifurcation points (ω in the ranges of 38–41·5 Hz) in order that the identified model can predict the bifurcation sequences more accurately.

4.1. CASE I

In this simple case, the induced voltage F_Φ is approximated by $F_\Phi = L_0(\mathrm{d}i/\mathrm{d}t)$, which implies that the inductance of the magnetic coil is treated as a constant value (L_0). The expression for the magnetic force which is a function of both the coil current and the air gap is approximated by a polynomial. Under these assumptions, equations (3) and (4) can be rewritten as

$$\frac{\mathrm{d}^2y}{\mathrm{d}t^2} + a_1\frac{\mathrm{d}y}{\mathrm{d}t} + a_2y + a_3y^2 + a_3y^3 + a_5i + a_6i^2 + a_7i^3 + a_0 = 0, \tag{5}$$

$$L_0\frac{\mathrm{d}i}{\mathrm{d}t} + iR = K_A A_0 \sin\omega t, \tag{6}$$

where i is the oscillating current about a biased current, and y is the oscillating displacement of the rotor about a reference point. Using the experimental data for $A_0 = 3{\cdot}0$ V, the identification technique mentioned in section 3 is carried out to determine the coefficients L_0, R and $a_{0\text{–}7}$ in equations (5) and (6), by applying the harmonic balance and the weighted least square method. The identified results are listed in Table 1. It is noted that if the order of magnitude of the parameters are significantly different from each other,

TABLE 1

Identified results for case I

	Identified values
a_1	41·418702
a_2	$2{\cdot}2779564 \times 10^4$
a_3	$3{\cdot}661201 \times 10^4$
a_4	$-0{\cdot}3566263 \times 10^6$
a_5	$0{\cdot}0622018 \times 10^5$
a_6	$-0{\cdot}2042933 \times 10^5$
a_7	$2{\cdot}734417 \times 10^4$
a_0	$0{\cdot}25324 \times 10^4$
L_0	0·0264988
R	9·7969308

the smallest parameter may have a larger percentage error due to the characteristics of the least square method. Under this situation, the concept of scaling can be applied to solve the problem caused by orders of magnitude.

Numerical simulations of equations (5) and (6) are performed by substituting the coefficients (Table 1) into equations (5) and (6) and letting $A_0 = 3{\cdot}0$ V. The resulting steady state responses in the range of 34–80 Hz along with the experimental data are presented in Figure 6. It is shown that the steady state displacement amplitude of this simple model can approximately follow the experimental data, with reasonable accuracy. However, the first period-doubling bifurcation appears near 34·1 Hz and the solution blows up when the frequency is decreased beyond 34 Hz. The period-doubling cascade and chaotic motion seen in the experimental data are absent in this model. This might be due to the fact that the assumption of the inductance (L_0) as a constant value introduces error in the estimation of inductance. Since the relationships between flux density (B) and magnetic field (H), and between F_m and i, are non-linear, the inductance will also depend on the operating point of the B–H diagram. This fact can be verified by drawing the inductance–current curve experimentally. The key work is to calculate the inductance at various bias voltages from

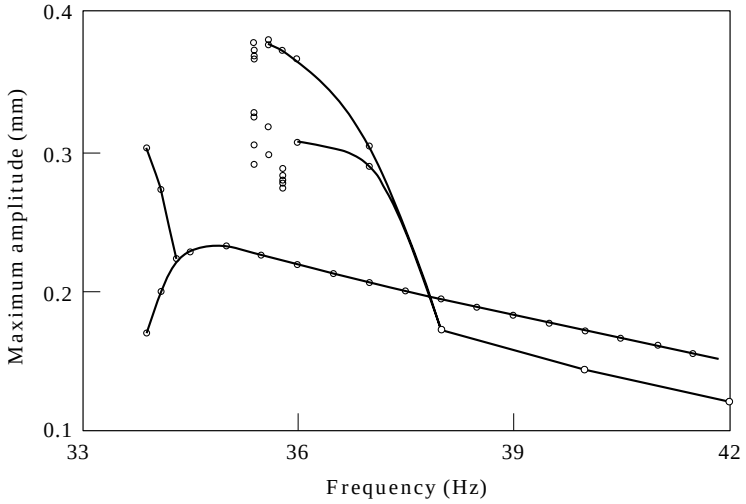

Figure 6. Comparison of bifurcation diagram obtained by experiment (○○○) and simulation (●●●) for case I.

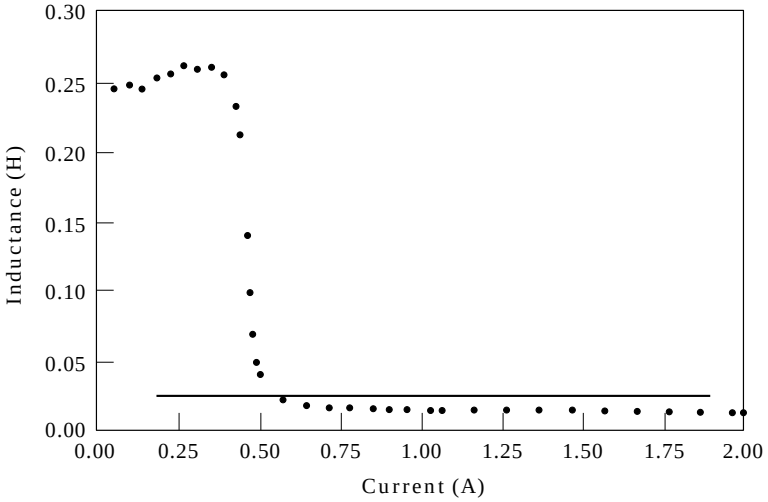

Figure 7. Inductance corresponding to various bias currents: experimental data (●●●) compared to the data estimated from case I (—).

0·2 to 6 V in steps of 0·2 V with the air gap of the rotor fixed at 0·44 mm. Then 26 small amplitude sinusoidal inputs with different frequencies (between 70 and 80 Hz) are superimposed on each bias voltage and the dynamic steady state response of coil current as well as the sinusoidal input are recorded simultaneously. Figure 7 shows the values of inductance corresponding to various bias voltages obtained by using these data and applying the identification technique mentioned above. It can be seen that the value of inductance does not remain constant. Rather, it varies as a function of the net coil current (I). If the coil current is kept within the regions $I < 0{\cdot}4$ A and $I > 0{\cdot}5$ A, then the value of inductance can be approximated to a constant value (average 0·254 H for $I < 0{\cdot}4$ A and 0·0167 H for $I > 0{\cdot}5$ A). However, the bias of the coil current in our case is 0·685 A and the oscillations (i) will inevitably go back and forth between these two regions. The estimation of inductance for this case results in $L_0 = 0{\cdot}0264988$ H. This value is acceptable for higher forcing frequency since the current i will be small. However, when the current i becomes larger on decreasing the forcing frequency, the estimated value of L_0 becomes too small compared to that of the physical system. This may be the primary reason for our observations shown in Figure 7 where the simple model introduces a relatively large error in amplitude when the current i gets larger.

4.2. CASE II

Once the characteristics of the inductance are known, techniques such as curve fitting can be applied to obtain a suitable form which will fit the experimental data perfectly. In this way, the simplest form of F_Φ in equation (4) to match the characteristics of the electromagnet is obtained as

$$F_\Phi = L_1(I_0 + i)^{-1}\frac{\mathrm{d}i}{\mathrm{d}t}, \tag{7}$$

where I_0 is the biased current measured directly from the average of experimental current time series and i is the oscillating current about I_0. Then the dynamic equations used to fit our physical system become.

$$\frac{d^2y}{dt^2} + a_1\frac{dy}{dt} + a_2y + a_3y^2 + a_4y^3 + a_5i + a_6i^2 + a_7i^3 + a_0 = 0, \tag{8}$$

$$L_1(I_0 + i)^{-1}\frac{di}{dt} + iR = K_A A_0 \sin \omega t, \tag{9}$$

Equation (8) is obtained in the same way as equation (5).

By using equations (8) and (9), similar identification calculations as in case I are performed. These results are displayed in Table 2. Using these coefficients, the frequency responses of equations (8) and (9) can be calculated and are shown by fine lines in Figure 8. From this figure, the steady state displacement amplitude of this model is shown to track the experimental data more closely than that in case I. The first period-doubling bifurcation is seen to occur at about 41·8 Hz and the period-doubling cascade and chaotic motion are shown to appear. But, the deviation of the bifurcation point of period-doubling bifurcation from that of the experimental data is quite notable (with relative error of 11·7%). Thus this model is still unacceptable.

Since the bifurcating behaviours belong to the characteristics of a highly non-linear system, the way of approximating the magnetic force in this simple form of polynomials may be inadequate for the physical system. To confirm this, a series of experiments were performed to find the relations among magnetic force, current, and displacement. Figure 9 illustrates the apparatus for this experiment. An electromagnet used in our physical system was fixed on a heavy seat and a rotor in short length was fixed on the dynamometer with a specified air gap between the electromagnet. The attractive forces sensing from the dynamometer (KISTLER 9257B) were recorded by the personal computer (PC) via a charge amplifier (KISTLER 5019A). Since the electromagnetic force was a function of both the air gap and the coil current, the test was performed by gradually increasing the current from zero to 2·0 A in steps of 0·25 A at various air gaps. The supplying currents were fed from a power amplifier and were metered previously by the PC. Since the nominal air gap of the control system was at 0·44 mm, five values of air gaps were selected in the tests, i.e., 0·3–0·5 mm in steps of 0·05 mm. At each stage, the histories of the current, air gap, and the magnetic force were recorded simultaneously. The experimental results are shown in Figure 10. From the diagram, it can be seen that the magnetic force is saturated when the coil current is increased beyond 0·3 A for various air gaps. As the coil current passes through this point, the magnetic force is quite insensitive to the increase of the coil current. It shows that the current-force relation of the electromagnet possesses highly non-linear characteristics. In our physical system, the

TABLE 2

Identified results for case II

	Identified values
a_1	41·418702
a_2	$2{\cdot}2779564 \times 10^4$
a_3	$3{\cdot}661201 \times 10^4$
a_4	$-0{\cdot}356623 \times 10^6$
a_5	$0{\cdot}0622018 \times 10^5$
a_6	$-0{\cdot}2042933 \times 10^5$
a_7	$2{\cdot}734417 \times 10^4$
a_0	$0{\cdot}25324 \times 10^4$
L_1	0·018096
R	9·7922279

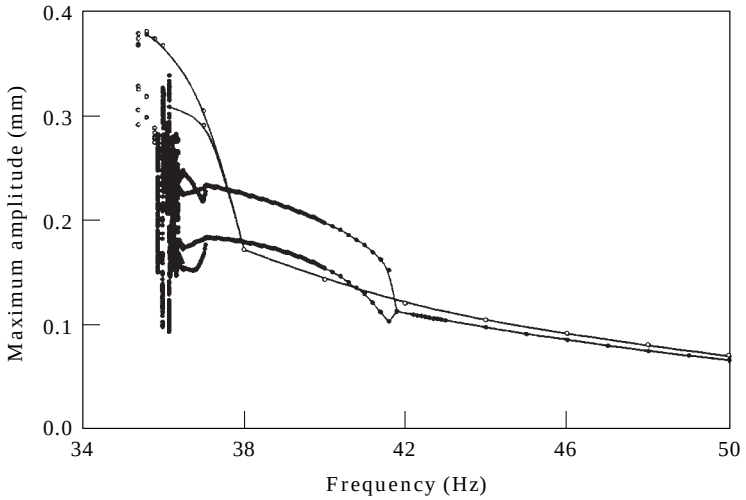

Figure 8. Comparison of bifurcation diagram obtained by experiment (○○○) and simulation for case II (●●●).

oepration point of coil current is biased at 0·685 A to levitate the rotor to the equilibrium position (with the nominal air gap 0.44 mm). When the oscillating amplitude of the coil current is increased, the magnetic force will be saturated such that the system exhibits rich dynamics.

4.3. CASE III

Having the experimental data for magnetic force at hand, the curve fitting procedures were performed to obtain two polynomials representing the force–current (fixed air gap) and force–air (fixed current) relations as follows.

$$F_1(I) = C_1 I^{2/3} + C_2 I^{4/3} + C_3 I^{6/3} + C_0, \qquad \text{with air gap fixed,} \tag{10}$$

$$F_2(\bar{y}) = D_1 \bar{y} + D_2 \bar{y}^2 + D_3 \bar{y}^3 + D_0, \qquad \text{with coil current fixed,} \tag{11}$$

where I is the total current including the biased current and the oscillating current input to the coil, and $\bar{y}$ is the air gap. Figure 11 shows the results of the curve fitting. In these figures, the non-linear terms in equations (10) and (11) can reasonably fit the experimental data. It is worth noting that although the addition of a larger number of parameters to describe the magnetic force may improve the accuracy of the approximation, the stochastic

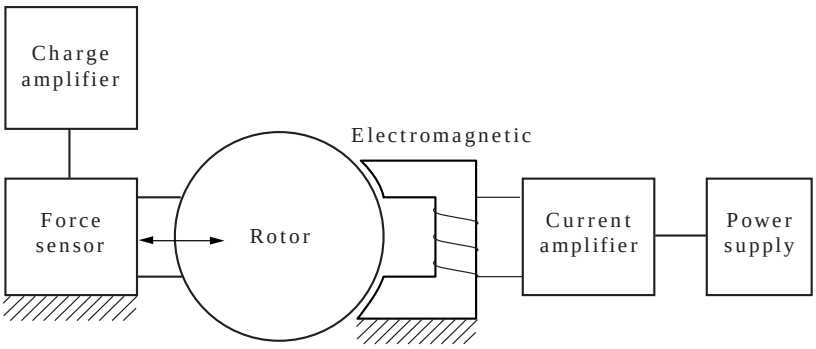

Figure 9. The apparatus for the magnetic force measurement.

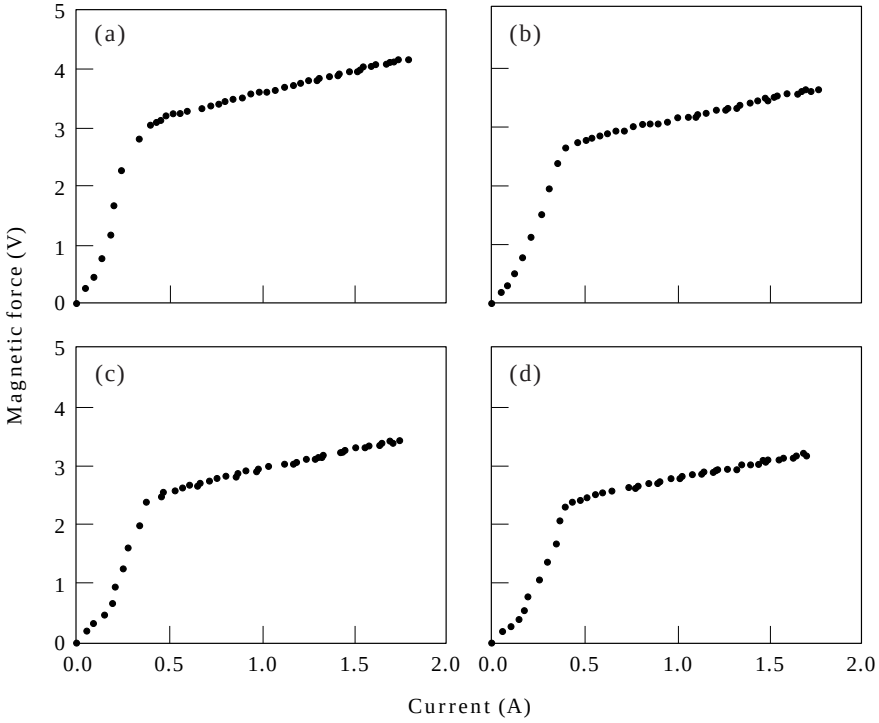

Figure 10. The magnetic force–current characteristics for various air gap: (a) 0·30 mm; (b) 0·40 mm; (c) 0·45 mm; (d) 0·50 mm.

error which is proportional to the number of parameters may increase accordingly in the subsquent identification calculations. Also note that since the magnetic force is a function of both the air gap and coil current when the rotor is in motion, the coefficients obtained by curve fitting cannot be substituted directly into equation (3) due to the fact that they are effective for fixed air gap or fixed current. Therefore, the curve fitting technique applied here is only to find the adequate non-linear terms to facilitate the identification.

Equations (10) and (11) are combined, with the current biased at operating point to represent the magnetic force ($F_m(i, y)$), so that equation (3) becomes

$$\frac{d^2y}{dt^2} + b_1\frac{dy}{dt} + b_2y + b_3y^2 + b_4y^3 + b_5(I_0 + i)^{6/3} + b_6(I_0 + i)^{2/3} + b_7(I_0 + i)^{4/3} + b_0 = 0, \tag{12}$$

$$L_1(I_0 + i)^{-1}\frac{di}{dt} + iR = K_A A_0 \sin \omega t, \tag{13}$$

where I_0 is the biased current calculated directly from the average of experimental current time series, and i is the oscillating current from I_0. Similarly, by using the experimental data and the harmonic balance method as in case II, the necessary coefficients (see Table 3) for equations (12) and (13) are obtained. Incorporating these results into equations (12) and (13) and letting $A_0 = 3{\cdot}0$ V, numerical simulations are carried out to obtain the simulated frequency response and to compare with the experimental data as shown in Figure 12. With this figure, it is first noticed that the steady state frequency response curve of this model is almost the same as that in case II. Second, as forcing frequency (ω) is

decreased, a cascade of period-doubling bifurcations are clearly seen which lead the system to chaos. The first period-doubling bifurcation point (about 39 Hz) is rather good in agreement with the experimental data (about 37·6 Hz), with relative error at about 3·7%.

In order to verify that the non-linear model of case III can capture the characteristic of the real system, the non-linear equations (12) and (13) are simulated to obtain two bifurcation curves, b_1 and b_2, and compared with the bifurcation curves, a_1 and a_2, which are obtained from experimental data. The results are shown in Figure 13. Similarly, the bifurcation curves c_1 and c_2 for case II obtained by simulating equations (8) and (9) are also shown in Figure 13 for comparison. In this figure, lines a_1 and a_2 are the bifurcation points of period-four and period-two, respectively, for various forcing amplitude (A_0) measured from the experimental data. If one starts at a high frequency and then decreases

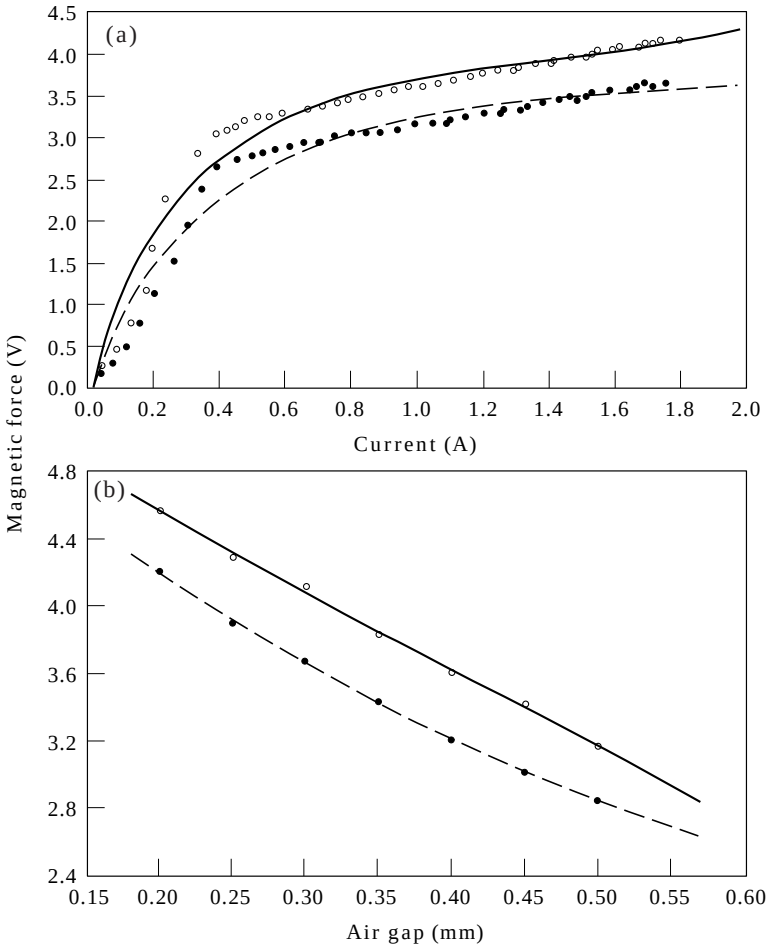

Figure 11. (a) Comparison of the magnetic force–current characteristics obtained by experiment and curve fitting for various air gaps. - - - , Curve fitting (equation (8)) with air gap = 0·40 mm; —, curve fitting (equation (8)) with air gap = 0·30 mm; ○ ○ , experiment with air gap = 0·30 mm; ● ●, experiment with air gap = 0·40 mm. (b) Comparison of the magnetic force–air gap characteristics obtained by experiment and curve fitting for various currents. - - - , Curve fitting (equation (9)) with coil current = 1·1 A; —, curve fitting (equation (9)) with coil current = 1·7 A; ○ ○ , experiment with coil current = 1·7 A; ● ●, experiment with coil current = 1·1 A.

TABLE 3

Identified results for case III

	Identified values
b_1	43·843782
b_2	$1{\cdot}7461747 \times 10^4$
b_3	$3{\cdot}969473 \times 10^4$
b_4	$-16{\cdot}80843 \times 10^4$
b_5	$3{\cdot}3106 \times 10^4$
b_6	$10{\cdot}505 \times 10^4$
b_7	$-9{\cdot}98479 \times 10^4$
b_0	$-3{\cdot}443392 \times 10^4$
L_1	0·018096
R	9·7922279

the forcing frequency slowly until it reaches line a_2 (in Figure 13) where a period-two bifurcation occurs, the T-period orbit loses stability and bifurcates into a period $2T$ orbit. Similarly, when the forcing frequency is decreased continuously until it meets line a_1 (in Figure 13) where a period-four bifurcation occurs, the $2T$-period orbit loses stability and bifurcates into a period $4T$ orbit. In other words, a period-two orbit exists in the region between line a_1 and line a_2. Line b_2 (period-two bifurcation curve) and line b_1 (period-four bifurcation curve) are obtained from case III. Line c_2 (period-two) bifurcation curve and line c_1 (period-four bifurcation curve) are obtained from case II. Clearly, the curves for period-two and period-four and thus chaotic motions predicted by case III are more in agreement with the experimental data than those by case II. Here the limited error existing in the figure can be considered to be caused by the approximations of the mathematical model.

In order to investigate the effectiveness and the relative contribution of the various terms of the polynomial form for the magnetic force applied in cases I, II and III, the current–force curve represented by this polynomial form is plotted to compare with that

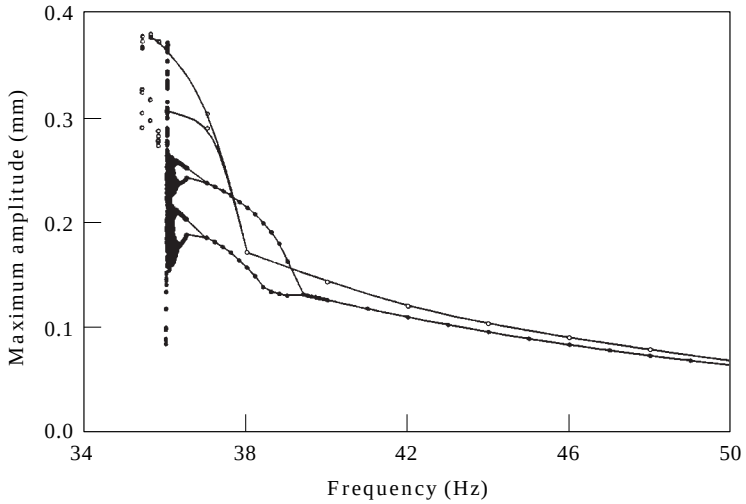

Figure 12. Comparison of bifurcation diagram obtained by experiment (○○○) and simulation for case III (●●●).

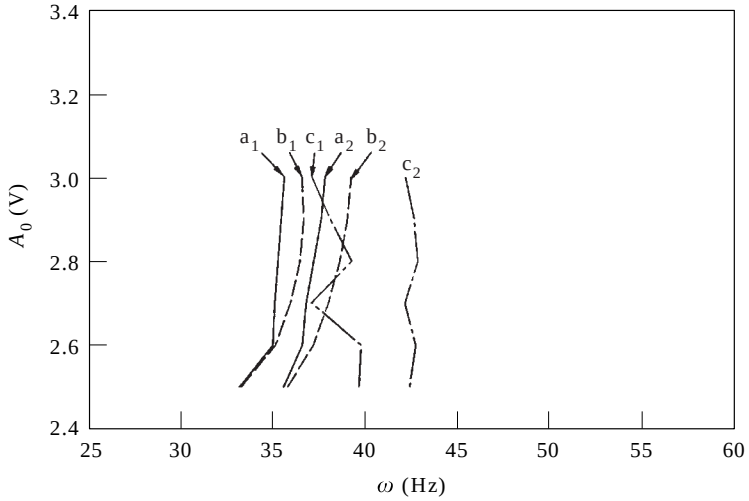

Figure 13. Period doubling bifurcation regions and their boundaries for various cases in the $A_0 - \omega$ space in decreasing driving frequency. Line a_1: period four bifurcation curve obtained by experiment; line b_1: period four bifurcation curve estimated from case III; line c_1: period four bifurcation curve estimated from case II; line a_2: period two bifurcation curve obtained by experiment; line b_2: period two bifurcation curve estimated from case III; line c_2: period two bifurcation curve estimated from case II.

of the experimental data. Figure 14(a) shows this diagram, where the magnetic forces have been normalized. It is clearly seen that the simple polynomial form (as case II) of the magnetic force matches the experimental data only in the vicinity of the operating point ($I_0 = 0{\cdot}685$ A). As the coil current goes far away from the bias current, the simple polynomial form is shown to deviate from the experimental data considerably. This may be the reason why equations (8) and (9) in case II fail to wholly capture the non-linear characteristics of our physical system. Figure 14(b) shows the comparison of normalized magnetic forces obtained experimentally and estimated by the various non-linear terms of case III. It can be seen that the magnetic force predicted by case III is more satisfactory. Thus, it can be concluded that this model successfully predicts the dynamic characteristics of the physical system.

In practice, the measured experimental data may contain a certain level of noise which complicates the identificating work. In order to study the effectiveness of this identification technique for signals containing noise, the random noise as shown in Figure 15(a) is added to the experimental time series for $A_0 = 3{\cdot}0$ V with ω ranging from 38 to 80 Hz. By applying these data and the identification procedure as before, the coefficients for equations (10) and (11) are obtained. Substituting the results into equations (10) and (11) and letting $A_0 = 3{\cdot}0$ V, the steady state frequency response is obtained, as shown in Figure 15(b). From this figure, we find that the steady state frequency response is almost the same as that of the experimental data without random noise. And the first period-doubling bifurcation point (about 39·5 Hz) is found to be in rather good agreement with the experimental data containing no random noise (about 39 Hz). This is due to using the "Discrete Fourier Transform" method in the identification calculations. The high-frequency noise will be filtered during the calculations. Therefore, this identification technique has proven to be effective in experimental data with small disturbed noise.

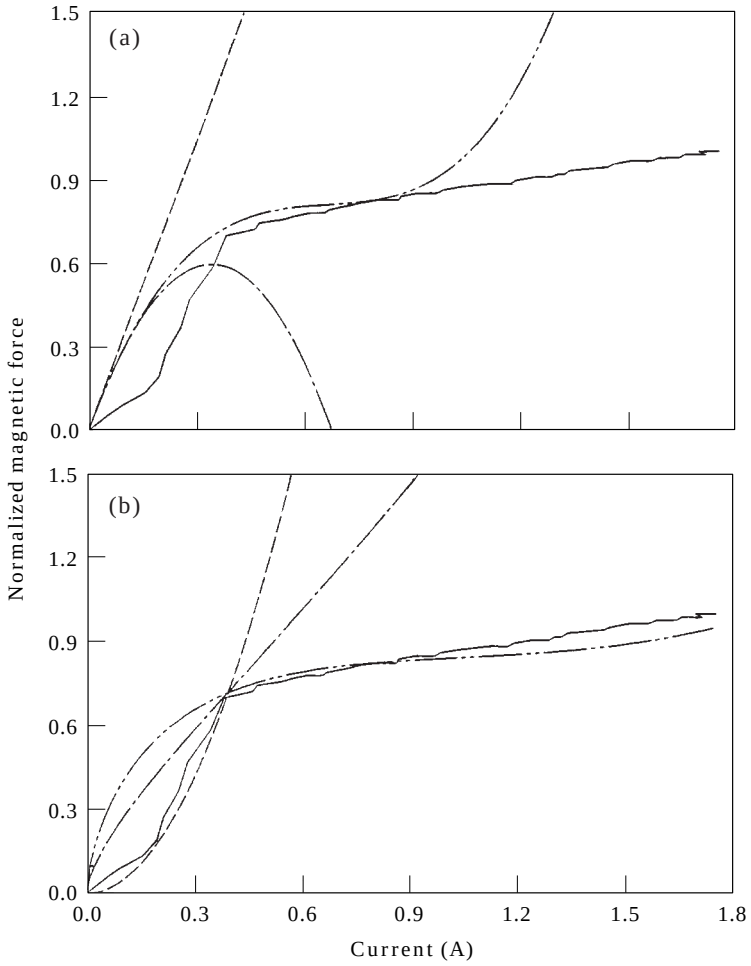

Figure 14. (a) Comparison of normalized force–current curves of the electromagnet obtained by experiment and estimation from case II: ——, experiment; — — —, no non-linear terms; — - — -, non-linear terms: y^2, i^2; —--—-—, non-linear terms: y^2, y^3, i^2, i^3. (b) Comparison of normalized force–current curves of the electromagnet obtained by experiment and estimation from case III: ——, experiment, — — —, non-linear terms: y^2, y^3, i^2; —-—-—, non-linear terms: y^2, y^3, i^2, $i^{2/3}$; : —--—-—, non-linear terms: y^2, y^3, i^2, $i^{2/3}$, $i^{4/3}$.

5. CONCLUSIONS AND REMARKS

In this paper, the curve fitting method was applied to fit the experimental data for fixed air gap and fixed coil current. The resulting functions, which are a function of both the air gap and the current, are combined to acquire the necessary non-linear terms to represent the non-linear magnetic force. Finally, the harmonic balance procedures and weighted least square method are performed to obtain the coefficients for these non-linear terms. With this modification, the proposed identification technique is proven to be more feasible in experiment.

From the experimental data, it was observed that this system contains rich non-linear phenomena. What mechanisms lead to such dynamics deserves to be further studied. This should be carried out by using the non-linear model obtained in case III and employing the advanced non-linear theory. Moreover, in the present study, only the dynamics of the

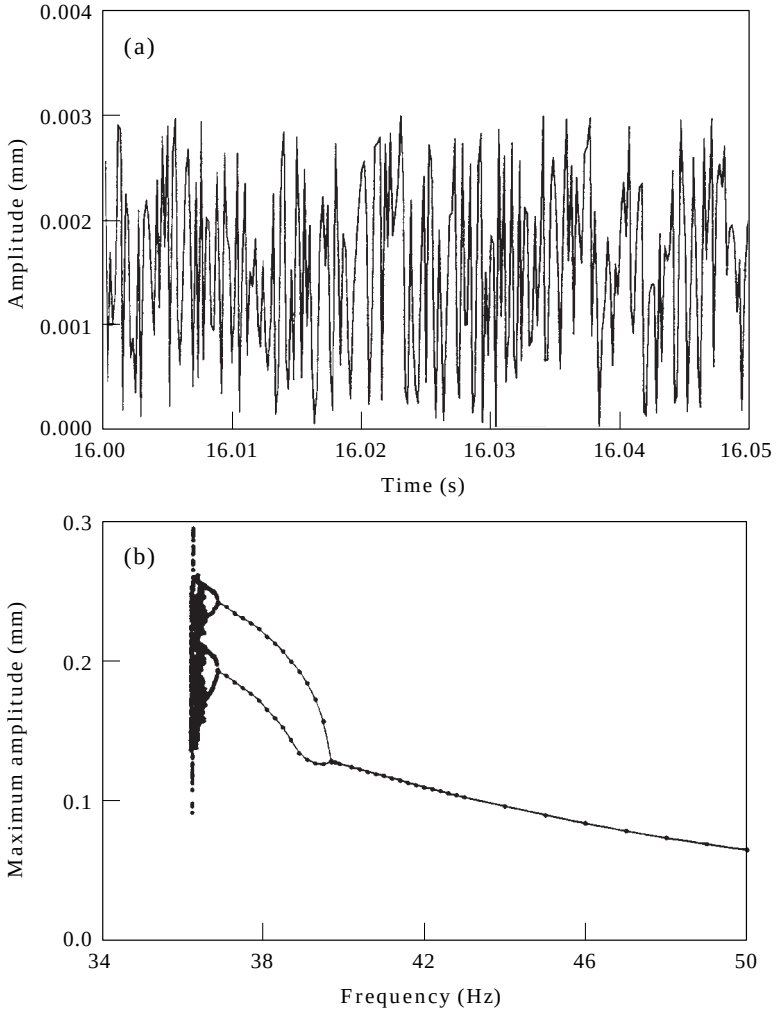

Figure 15. (a) Random noise. (b) Bifurcation diagram obtain by case III with random noise.

system in the vertical direction is investigated. When the rotor is rotated, the coupling effects between the vertical and horizontal directions, especially at high rotating speed and a large disturbed amplitude, may become significant. In such a situation, the following should be noted in identification calculations. (1) All the magnetic forces of the electromagnet in the assuming model should be a function of the current and the air gaps of both vertical and horizontal directions. (2) The gyroscopic effects associated with the spinning rotor should be considered. (3) The identification procedure for this situation will be the same as that applied in this paper, but will be more complicated. Identifying a model to capture the dynamics of the system under this situation is our forthcoming work.

REFERENCES

1. C. K. Sortore *et al*. 1990 *Proceedings of the Second International Symposium on Magnetic Bearings*. Permanent magnet biased magnetic bearings—design, construction and testing.

2. F. C. Moon and Y. H. Pao 1969 *American Society of Mechanical Engineers*, *Journal of Applied Mechanics* **36**, 92–100. Vibration and dynamic instability of a beam–plate in a transverse magnetic field.
3. J. Gertler and C. Banyasz 1974 *IEEE Transactions on Automatic Control* **19**, 816–820. A recursive (on-line) maximum likelihood identification method.
4. T. C. Hsia 1976 *IEEE Transactions on Automatic Control* **21**, 104–108. Least square alogrithim for system parameter identification.
5. B. M. Finigan and I. H. Rowe 1974 *IEEE Transactions on Automatic Control* **19**, 825–830. Strongly consistent parameter estimation by the introduction of strong instrumental variables.
6. P. Ibanze 1975 *Journal of Nuclear Engineering and Design* **25**, 30–41. Identification of dynamic parameters of linear and nonlinear structural models from experimental data.
7. J. G. Beliveau 1976 *American Society of Mechanical Engineers*, *Journal of Applied Mechanics* **43**, 335–339. Identification of Viscous damping in structures from model information.
8. S. F. Masri and T. K. Caughey 1976 *American Society of Mechanical Engineers*, *Journal of Applied Mechanics* **46**, 433–447. A nonparametric identification technique for nonlinear dynamic problems.
9. F. E. Udwadia and C. P. Kuo 1981 *Earthquake Engineer and Structural Dynamics* **9**, 385–409. Non-parametric Identification of a class of non-linear close-coupled dynamic systems.
10. Y. Yang and S. R. Ibrahim 1985 *American Society of Mechanical Engineers*, *Journal of Vibration*, *Acoustics*, *Stress*, *and Reliability in Design* **107**, 60–66. Nonparametric identification technique for a variety of discrete non-linear vibrating systems.
11. K. Yasuda and S. Kawamura 1989 *International Journal Series III* **32**, 365–372. A nonparametric identification technique for vibratory systems (proposition of the technique).
12. K. Yasuda, S. Kawamura and S. Watanabe 1988 *International Journal Series III* **31**, 8–14. Identification of non-linear multi-degree-of-freedom systems (presentation of an identification technique).
13. J. H. Wang and C. M. Liou 1991 *American Society of Mechanical Engineers*, *Journal of Vibration*, *Acoustics*, *Stress*, *and Reliability in Design* **107**, 28–35. Experimental identification of mechanical joint parameters.
14. Y. Y. Zhang, Y. B. Xie and D. M. Qie 1992 *Journal of Sound and Vibration* **152**, 549–559. Identification of linearized oil–film coefficients in a flexible rotor-bearing system, part II: experiment.
15. P. Arumugam, S. Swarnamani and B. S. Prabhu 1995 *American Society of Mechanical Engineers*, *Journal of Engineering for Gas Turbines and Power* **117**, 593–599. Experimental identification of linearized oil film coefficients of cylindrical and tilting pad bearings.
16. K. Yi and K. Hedrick 1995 *American Society of Mechanical Engineers*, *Journal of Dynamic System*, *Measurement*, *and Control* **117**, 175–182. Observer-based identification of nonlinear system parameters.
17. J. X. Zhang and J. B. Roberts 1996 *Journal of Sound and Vibration* **189**, 173–191. A frequency Domain parametric identification method for studying the non-linear performance of squeeze-film dampers.
18. R. Johansson 1993 *System Modeling and Identification*. Englewood Cliffs, NJ: Prentice-Hall.